Vietnam Journal of Science and Technology ***60*** *(3) (2022) 458-467*

doi:10.15625/2525-2518/16330

HARD MAGNETIC PROPERTY OF Mn-Ga-Al MELT-SPUN RIBBONS

Pham Thi Thanh[1, 2, *], Nguyen Mau Lam[3], Dinh Thi Kim Oanh[2], Nguyen Huy Ngoc[1, 2], Kieu Xuan Hau[1, 2], Nguyen Hai Yen[1, 2], Truong Viet Anh[4], Vu Manh Quang[3], Nguyen Thi Nguyet Nga[5], Nguyen Huy Dan[1, 2]

[1]*Institute of Materials Science, Vietnam Academy of Science and Technology, 18 Hoang Quoc Viet, Ha Noi, Viet Nam*

[2]*Graduate University of Science and Technology, Vietnam Academy of Science and Technology, 18 Hoang Quoc Viet, Ha Noi, Viet Nam*

[3]*Hanoi Pedagogical University 2, 32 Nguyen Van Linh, Xuan Hoa, Phuc Yen, Vinh Phuc, Viet Nam*

[4]*Hanoi University of Science and Technology, 1 Dai Co Viet, 100000 Ha Noi, Viet Nam*

[5]*Hung Vuong University, Nong Trang, 290000 Phu Tho, Viet Nam*

[*]Email: *thanhpt@ims.vast.ac.vn*

Received: 31 July 2021; Accepted for publication: 24 March 2022

Abstract. Mn-Ga-based alloy system has exhibited hard magnetic properties, although this alloy system contains no rare earth elements. However, magnetic parameters of Mn-Ga alloys have not yet been comparable to those of rare earth magnets such as Nd-Fe-B, Sm-Co, etc. Therefore, enhancement of the magnetic properties of the Mn-Ga-based alloys has interestingly been researched by scientists in the world. Partial replacement of both the Ga and Mn by other elements (Al, Cu, Bi, Cr, etc.) with suitable synthesis conditions (annealing temperature, annealing time, etc.) have shown improvement in the magnetic properties of the Mn-Ga-based alloys. In this paper, we investigated the effect of Al concentration and annealing conditions on the structure and magnetic properties of $Mn_{65}Ga_{25-x}Al_{10+x}$ (x = 0, 5 and 10) alloy ribbons prepared by melt-spinning method. Crystalline phases of MnAl, $D0_{19}$-type Mn_3Ga and $D0_{22}$-type Mn_3Ga were found in all the ribbons. The $D0_{22}$-type Mn_3Ga hard magnetic phase is dominated by appropriate Al concentration and annealing conditions. Coercivities, H_c, greater than 10 kOe were achieved on the alloys at an optimal annealing temperature and time of 650 ^oC and 1 h, respectively. The obtained results show applicability of the Mn-Ga-based alloys as a new kind of rare earth-free hard magnetic materials in applications.

Keywords: Coercive mechanism, rare earth-free magnets, hard magnetic materials, melt-spinning method.

Classification numbers: 2.2.1.

1. INTRODUCTION

Due to the increasing demand for hard magnetic materials in modern life (motors, generators, computers, phones, cars, refrigerators, etc.) and the limited availability of resource and exploitation, rare earth elements have their cost soar and become national strategy materials. Therefore, producing rare earth-free hard magnetic materials with their features meeting the application requirements will avoid high costs and uncertain rare earth supplies. Recent studies around the world have shown a great potential for practical applications of a new generation of rare earth-free hard magnetic materials [1-7]. Besides, rare earth-free hard magnetic materials have other advantages (stability, easy processing, etc.) that rare-earth-containing materials do not have. Among them, Mn-based magnets (Mn-Bi, Mn-Al and Mn-Ga) have attracted the attention of many researchers [8-16]. Especially, with Curie temperature above room temperature and high magnetic anisotropy, Mn-Ga magnets have many application potentials for magnetoelectronic equipments [17-20]. There are some methods such as melt-spinning, arc-melting, high-energy mechanical milling, etc. which are used to fabricate Mn-Ga magnets in various forms (bulk, ribbon, nanocomposites, etc.). Among these methods, the melt-spinning method is the most important because it can be easily used to produce a large amount of materials for practical applications. It is well known that, the magnetic properties of materials are strongly sensitive to their microstructure, which is determined by composition and fabrication conditions. The rapid quenching method can create the desired microstructure in combination with the annealing process. That means the desired structure formation can be easily controlled by technological conditions. Therefore, melt-spinning is an appropriate method to fabricate Mn-Ga-based materials.

Previous studies have shown that the phase formation in Mn-Ga-based alloys is rather complicated [21 - 23]. The Mn_3Ga phase is formed with various types of crystalline structures including tetragonal ($L1_0$), hexagonal ($D0_{19}$), tetragonal ($D0_{22}$) and cubic (disordered Cu_3Au-type structure). The formation of these crystalline phases depends on elemental compositions and annealing conditions. The hexagonal $D0_{19}$ and the tetragonal $D0_{22}$ are two phases which appear crucially in Mn-Ga magnets. At room temperature, the $D0_{19}$-type Mn_3Ga phase is antiferromagnetic, which is easily formed because of its stability. Meanwhile, the $D0_{22}$-type Mn_3Ga ferromagnetic phase, which has low saturation magnetization (M_s = 110 emu/cm^3), high perpendicular anisotropy with a uniaxial anisotropy constant of K_u = 0.89 MJ/m^3 and high Curie temperature (T_C = 765 K) plays an important part in the hard magnetic properties of Mn-Ga magnets [24, 25]. As reported in [26, 27], the hard magnetic phases in Mn-Ga binary alloys are usually formed with long annealing time. So far, magnetic parameters of Mn-Ga melt-spun ribbons, especially their coercivity, have not yet been comparable to those of rare earth-based permanent magnets. Therefore, moreover enhancement of magnetic properties of this kind of magnets is still in focus for research. Previous works [28 - 33] indicated that the coercivity of Mn-Ga magnets can reach over 10 kOe by the addition of a small amount of Al, Cr, Fe, Cu, etc. Magnetic properties of these magnets are also significantly enhanced by applying appropriate technological conditions such as intermediate phase creating, interrupt-annealing, multi-annealing, etc. Saito T. *et al*. reported that the coercivity of $Mn_{65}Ga_{15}Al_{20}$ ribbons annealed at 700 ^{o}C for 1 h increased from 5 to 9 kOe [29]. Partial replacement of Ga by Al forms a new cubic phase, which improves the hard magnetism of the sample. At the same time, Al also reduces the particle size, which is generally better for generating high coercivity. As for Cu addition, the coercivity reached 20 kOe for the bulk $Mn_{55.2}Ga_{19}Cu_{25.8}$ alloy annealed at 800 ^{o}C for 24 h [30]. The formation of Cu-rich nonmagnetic boundary phase creates magnetic isolation for the matrix region or pinning sites for magnetic domain walls leading to high coercivity. In another research [32], by adding Cr to the milled Mn_3Ga compound, a new Cr_3Ga_4 binary phase is obtained. Annealing at 350 ^{o}C for 60 h changes the crystalline phases of the material and

affects its magnetic properties. The obtained results show that the saturation magnetization increases but the coercivity decreases.

In this work, the nonmagnetic Al element was selected to partially replace Ga in alloys prepared by rapid quenching method to further improve their coercivity. The influence of Al concentration and annealing process on the structure and magnetic properties of $Mn_{65}Ga_{25-x}Al_{10+x}$ (x = 0, 5 and 10) alloy ribbons was investigated.

2. EXPERIMENTAL

Pre-alloys with nominal composition $Mn_{65}Ga_{25-x}Al_{10+x}$ (x = 0, 5 and 10) were prepared from pure metals Mn, Ga and Al on an arc-melting furnace. Because Mn is evaporated during arc-melting, an excess of 15 wt.% of Mn was added to the nominal composition. This compensation amount of Mn was determined based on the loss of about 3 wt.% of Mn after each time of arc-melting under the same preparation conditions and each sample was arc-melted five times to ensure homogeneity. After arc-melting, the pre-alloys were used to fabricate ribbons on a melt-spinning system at the same tangential velocity, v = 20 m/s, of the copper roller. The obtained ribbons were annealed at various temperatures of 550 ^oC, 600 ^oC, 650 ^oC, 700 ^oC and 750 ^oC for 1 h. All the arc-melting, melt-spinning and annealing processes were performed under Ar atmosphere to avoid oxygenation process. The structure of the materials was analyzed by X-ray diffraction method on an Equinox 5000 - Thermo Scientific instrument with Cu-K_α radiation source (λ = 1.5406 Å). The magnetization measurements on both the pulsed field and vibrating sample magnetometers were used to investigate the magnetic properties of the samples.

3. RESULTS AND DISCUSSION

XRD patterns of the as-quenched $Mn_{65}Ga_{25-x}Al_{10+x}$ (x = 0, 5 and 10) ribbons with a thickness of 45 μm are shown in Figure 1a. The structure of all the ribbons is similar. Their XRD patterns manifest a multiphase structure. The diffraction peaks appearing on the XRD patterns correspond to MnAl, $D0_{22}$-type Mn_3Ga and $D0_{19}$-type Mn_3Ga phases. However, the diffraction peaks of MnAl phase are dominant. The intensity of the MnAl peaks increases with increasing Al concentration from 10 % (x = 0) to 20 % (x = 10). At 2θ angle of 41.5^o, there is a superposition of two diffraction peaks corresponding to the crystalline phases of MnAl and $D0_{19}$-type Mn_3Ga. Only one diffraction peak corresponding to the $D0_{22}$-type Mn_3Ga phase is found for the as-quenched ribbons with all the concentrations of Al. On the other hand, the intensity of the $D0_{22}$-type Mn_3Ga characteristic peaks is very weak, i.e. the volume fraction of this phase in the as-quenched ribbons is small. As mentioned in the introduction section, the $D0_{22}$-type Mn_3Ga crystalline phase is a ferromagnetic phase that causes high coercivity for Mn-Ga based alloys. The crystalline structure of this alloy system is very susceptible to change. During the annealing process, in addition to the increasing fraction of crystalline phase, the atoms also diffuse and replace other positions in the lattice cell. Therefore, the lattice constant can be changed leading to the displacement of diffraction peaks. In order to enhance the volume fraction of this hard magnetic crystalline phase, the ribbons were annealed under various conditions to obtain the optimal structure for the material. The annealing temperature, T_a, was varied from 550 to 750 ^oC and the annealing time, t_a, was kept for 1 h.

Figure 1b shows XRD patterns of the $Mn_{65}Ga_{25-x}Al_{10+x}$ ribbons annealed at 650 ^oC for 1 h. We can see that, the crystalline phases are significantly changed after annealing process. The intensity of the diffraction peaks of all the crystalline phases is sharper after annealing. That

means the crystalline phases are recrystallized from the amorphous phase in the alloy ribbons. However, the recrystallization of the crystalline phases is different. The number of diffraction peaks characterizing the $D0_{22}$-type Mn_3Ga phase increases clearly after annealing. On the other hand, the intensity of these $D0_{22}$-type Mn_3Ga peaks is also increased. It should be noted that when the concentration of Al is increased from 10 % to 20 %, the $D0_{22}$-type Mn_3Ga crystalline phase dominates and reaches its maximal volume fraction at 15 % of Al. Daniel R. B. *et al.* have shown that the formation of this phase can be beneficial for the hard magnetic property of the material [20]. Thus, annealing process for Mn-Ga based ribbons is an effective method to enhance the $D0_{22}$-type Mn_3Ga phase. Selecting the optimal annealing regime will limit the formation of undesired phases. The recrystallization of the crystalline phases during annealing affects the magnetic properties of the alloy ribbons. Figure 2 shows hysteresis loops of the as-quenched $Mn_{65}Ga_{25-x}Al_{10+x}$ (x = 0, 5 and 10) ribbons. The coercivity and saturation magnetization are rather small, below 0.6 kOe (see the inset of Figure 2) and 1.5 emu/g, respectively for the as-quenched ribbons. The magnetization in the magnetic field H = 12 kOe, M_{12kOe}, decreases when increasing x from 0 to 10. Meanwhile, the coercivity reaches its maximal value with x = 5.

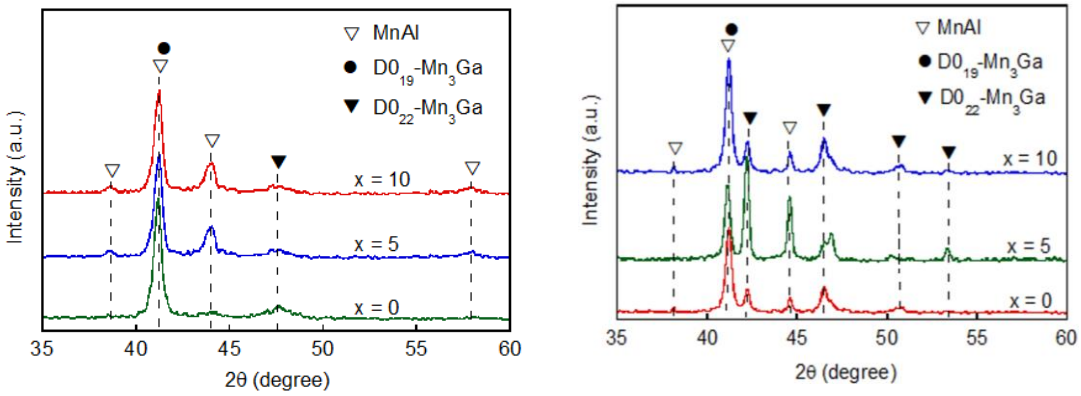

a) b)

Figure 1. XRD patterns of the as-quenched (a) and annealed (b) $Mn_{65}Ga_{25-x}Al_{10+x}$ (x = 0, 5 and 10) ribbons.

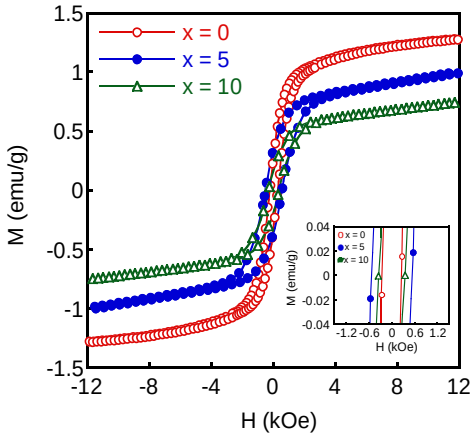

Figure 2. Hysteresis loops of the as-quenched $Mn_{65}Ga_{25-x}Al_{10+x}$ (x = 0, 5 and 10) ribbons. The inset is the enlarged hysteresis loops in low external magnetic field range.

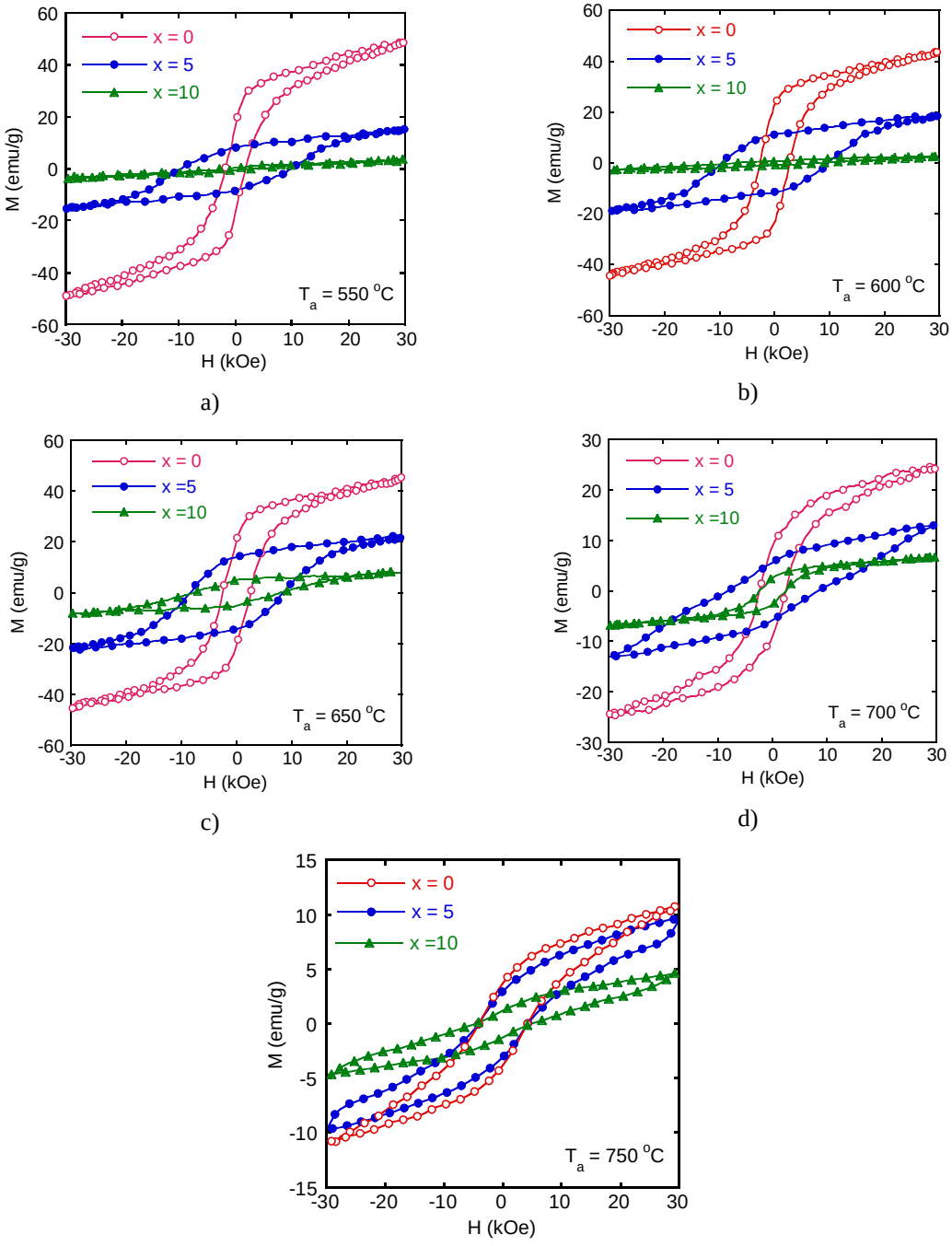

Figure 3. Hysteresis loops of the $Mn_{65}Ga_{25-x}Al_{10+x}$ (x = 0, 5 and 10) ribbons annealed at various temperatures of 550 °C (a), 600 °C (b), 650 °C (c), 700 °C (d), and 750 °C (e) for 1 h.

Hysteresis loops of the $Mn_{65}Ga_{25-x}Al_{10+x}$ ribbons annealed at 550 °C, 600 °C, 650 °C, 700 °C and 750 °C for 1 h are shown in Figure 3. We can realize that the annealing temperature clearly

affects the magnetic properties of the alloys. The hysteresis loop of all the samples greatly expands after annealing at all temperatures. That means the phase, which characterizes the hard magnetic property of the material, was formed during the annealing process resulting in an increase in the coercivity of the ribbons. Both the coercivity and magnetization of the samples are significantly increased after annealing. H_c increases above 10 kOe for the sample with x = 5 and the saturation magnetization exceeds 50 emu/g for the sample with x = 0. Thus, ferromagnetic behavior is developed in the annealed samples. This is in good concordance with the obtained results from the XRD patterns in Figure 1b. The volume fraction of the $D0_{22}$-type Mn_3Ga phase considerably increases after annealing process. The highest coercivity was achieved on the sample with the maximal volume fraction of the $D0_{22}$-type Mn_3Ga phase. The saturation magnetization of the samples was also observed to depend on the annealing process. With appropriate annealing regimes and concentrations of Al, the saturation magnetization of the alloys can be increased tens of times compared to that of the as-quenched ones.

Figure 4 shows the dependence of coercivity, H_c, and saturation magnetization, M_s, of the samples on annealing temperature. We can see that with increasing annealing temperature from 550 ^oC to 750 ^oC, the saturation magnetization of the sample with x = 5 decreases monotonically, while this quantity of the samples with x = 5 and x = 10 reaches the maximum value at 650 ^oC. However, the saturation magnetization of all the samples annealed at temperature of 650 °C do not change much compared to those annealed at lower temperatures. In general, the saturation magnetization of the alloys with all the investigated concentrations of Al can be significantly enhanced by annealing at 650 °C. The highest saturation magnetization of 50.8, 18.6 and 6.2 emu/g was obtained for the alloy with Al concentrations of 10 %, 15 % and 20 %, respectively. As for the coercivity, its variation with Al concentration is different from that of the saturation magnetization. From Figure 4b, we can see that the coercivity of the ribbons is greatly enhanced when the concentration of Al increases from 10 % to 15 %. On the other hand, each of the alloys with different concentrations of Al has its own optimal annealing temperature, where the crystalline structure of the alloys is optimally formed leading to the best performance for the hard magnetic material. For example, the alloys with x = 0 and 5 have the optimal annealing temperature of 650 ^oC and their highest coercivity is 6.2 kOe and 10.5 kOe, respectively. When the annealing temperature is higher than 650 ^oC, not only fraction of the crystalline phase but also the grain size increases rapidly, exceeding the size of single domain (optimal for coercivity), leading to a decrease in coercivity. Meanwhile, the highest coercivity of 7.7 kOe for the sample with x = 10 was obtained at the optimal annealing temperature of 600 ^oC. The obtained results are in good agreement with the study of Saito T. *et al*. [25]. The opposite variation trends of the coercivity and the saturation magnetization can be explained as follows. When the volume fraction of the $D0_{22}$-type Mn_3Ga ferromagnetic phase increases, the coercivity of the alloy is enhanced. As the $D0_{19}$-type Mn_3Ga antiferromagnetic phase increases, the saturation magnetization of the alloy is reduced. The formation of these two crystalline phases depends on Al concentration and annealing temperature. For the $D0_{19}$-type Mn_3Ga antiferromagnetic crystalline phase, its volume fraction increases with Al concentration. Therefore, the saturation magnetization of the alloy decreases as the Al concentration increases. As for the $D0_{22}$-type Mn_3Ga ferromagnetic phase, its volume fraction is maximized with an Al concentration of 15 % (x = 5) leading to the maximum coercivity of the alloy. In order to obtain both high saturation magnetization M_s and coercivity H_c, it is necessary to simultaneously increase the phases with high H_c and M_s. That means to reduce the formation of antiferromagnetic phase with low H_c and M_s. On the other hand, controlling the particle size of the hard magnetic phase increases H_c without reducing M_s.

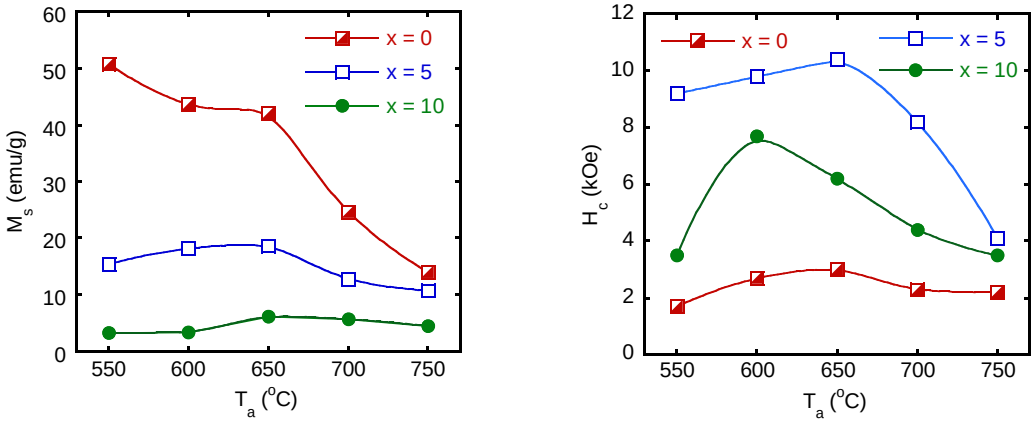

Figure 4. Dependence of saturation magnetization M_s (a) and coercivity H_c (b) on annealing temperature T_a of the $Mn_{65}Ga_{25-x}Al_{10+x}$ (x = 0, 5 and 10) alloys.

Table 1. Comparison of the magnetic properties of the $Mn_{65}Ga_{25-x}Al_{10+x}$ (x = 0, 5 and 10) alloy ribbons studied in this work with those of the previously reported Mn-Ga added magnets.

Nominal composition	v (m/s)	T_a (°C)	t_a (h)	M_s (emu/g)	H_c (kOe)	Reference
$Mn_{65}Ga_{25}Al_{10}$	20	650	1	50.8	1.7	This work
$Mn_{65}Ga_{20}Al_{15}$	20	650	1	20	10.5	This work
$Mn_{65}Ga_{15}Al_{20}$	20	650	1	6.2	7.7	This work
$Mn_{65}Ga_{35}$	40	300	1	-	2.5	[31]
$Mn_{65}Ga_{30}Cu_5$	40	300	1	-	5.6	[31]
$Mn_{65}Ga_{25}Cu_{10}$	40	300	1	-	15.7	[31]
$Mn_{65}Ga_{20}Cu_{15}$	40	300	1	-	2.2	[31]
$Mn_{65}Ga_{15}Cu_{20}$	40	300	1	-	1.7	[31]
$Mn_{65}Ga_{30}Al_5$	50	700	1	28	4.7	[29]
$Mn_{65}Ga_{25}Al_{10}$	50	700	1	31	3.1	[29]
$Mn_{65}Ga_{20}Al_{15}$	50	700	1	18	7.5	[29]
$Mn_{65}Ga_{15}Al_{20}$	50	700	1	11	9.1	[29]
$Mn_{65}Ga_{10}Al_{25}$	50	700	1	9	4.9	[29]

Table 1 shows a comparison of the magnetic properties of the alloy ribbons in this work and the previously reported Mn-Ga added magnets. Each composition has its own optimal technological conditions and different magnetic parameters. Our obtained results show that the values of H_c and M_s are quite high compared with those of the same composition from other research groups.

4. CONCLUSIONS

The influence of Al concentration and annealing process on the structure and magnetic properties of the $Mn_{65}Ga_{25-x}Al_{10+x}$ (x = 0, 5, and 10) ribbons was investigated. The formation of the $D0_{22}$-type Mn_3Ga hard magnetic phase is strongly dependent on both Al concentration and annealing temperature. The highest saturation magnetization of 50.8 emu/g is obtained for the alloy with an Al concentration of 10 at%, while the coercivity reaches a maximal value of 10.5 kOe with an Al concentration of 15 at%. In general, annealing at 650 ^oC for 1 h is optimal for the alloys.

Acknowledgements. This research is funded by the National Foundation for Science and Technology Development (NAFOSTED) of Viet Nam under grant number of 103.02-2018.339. A part of the work was done in the Key Laboratory for Electronic Materials and Devices and Laboratory of Magnetism and Superconductivity, Institute of Materials Science, Viet Nam.

CRediT authorship contribution statement. Pham Thi Thanh: Curation data, Writing original draft. Nguyen Mau Lam, Nguyen Huy Ngoc, Truong Viet Anh, Dinh Thi Kim Oanh: Fabricating samples. Kieu Xuan Hau, Vu Manh Quang, Nguyen Thi Nguyet Nga: Measurement. Nguyen Hai Yen: Analysis data. Nguyen Huy Dan: Supervision, Revising manuscript.

Declaration of competing interest. The authors declare that they have no known competing financial interests or personal relationships that could have appeared to influence the work reported in this paper.

REFERENCES

1. Jun C., Matt K., Lin Z., Fei Liu, Alexander G., George H., Balamurugan B. and David S. - Current progress and future challenges in rare-earth-free permanent magnets, Acta Mater. **158** (2018) 118-137. https://doi.org/10.1016/j.actamat.2018.07.049.
2. Xuan Z., Zhongwu L., Hongya Y., Hui Z. and Guoqing Z. - Optimization of rapidly quenched Co–Zr and (Co,Fe)–Zr alloys for rare earth free permanent magnets, Phys. B Condens. Matter. **599** (2020) 412549. https://doi.org/10.1016/j.physb.2020.412549.
3. Brandt A. J., Wei T., Xubo L., Alexandra I. N., Gaoyuan O., Kevin W. D. and Jun C. - Optimizing composition in MnBi permanent magnet alloys, Acta Mater. **181** (2019) 595-602. https://doi.org/10.1016/j.actamat.2019.10.003.
4. Chang H. W., Liao M. C., Shih C. W., Chang W. C., Yang C. C., Hsiao C. H. and Ouyang H. - Hard magnetic property enhancement of Co_7Hf-based ribbons by boron doping, Appl. Phys. Lett. **105** (2014) 192404. https://doi.org/10.1063/1.4901737.
5. Goto S., Kura H., Watanabe E., Hayashi Y., Yanagihara H., Shimada Y., Mizuguchi M., Takanashi K. and Kita E. - Synthesis of single-phase $L1_0$-FeNi magnet powder by nitrogen insertion and topotactic extraction, Sci. Rep. **7** (2017) 13216. https://doi.org/10.1038/s41598-017-13562-2.
6. Lyubina J., Gutfleisch O., Muller K. H. and Schultz L. and Dempsey N. M. - Nanocrystalline hard magnetic FePt powders, J. Appl. Phys. **95** (2004) 7474-7476. https://doi.org/10.1063/1.1652393.
7. Goyal R., Arora N., Kapoor A., Lamba S. and Annapoorni S. - Exchange hardening in $FePt/Fe_3Pt$ dual exchange spring magnet: Monte Carlo modeling, J. Alloys Comp. **695** (2017) 1014-1019. https://doi.org/10.1016/j.jallcom.2016.10.224.

8. Volegov A. S., Muller K. H., Bittner F., Mix T., Neznakhin D. S., Volegova E. A., Schultz L., Woodcock T. G. and Nenkov K. - Magnetic viscosity of $L1_0$ structured Mn-Ga and Mn-Al alloys, J. Magn. Magn. Mater. **441** (2017) 750-756.

http://dx.doi.org/10.1016/j.jmmm.2017.06.087.

9. Wei J. Z., Wu R., Yunbo Y., Xuegang C., Yuanhua X., Yang Y. C., Changsheng W. and Jinbo Y. Structural properties and large coercivity of bulk $Mn_{3-x}Ga$ ($0 \leq x \leq 1.15$), J. Appl. Phys. **115** (2014) 17A736. https://doi.org/10.1063/1.4866844 .
10. Zhengying J., Yuxiao J., Bochen L., Jingmin W. and Chengbao J. - Microstructure and magnetic properties of $(Mn_{54}Al_{46})_{98}C_2$ magnets fabricated by liquid-phase sintering with the $Mn_{65}Ga_{35}$ as an additive, J. Magn. Magn. Mater. **534** (2021) 168037. https://doi.org/10.1016/j.jmmm.2021.168037.
11. Alina D. C., Aurel L., Cristina B., Ioan D. and Ovidiu C. - Magnetism and ε-τ Phase Transformation in MnAl-Based Nanocomposite Magnets, Nanomaterials **11** (2021) 896-909. https://doi.org/10.3390/nano11040896.
12. Zhongwu L., Chen C., Zheng Z. G., Tan B. H. and Raju V. R. - Phase transitions and hard magnetic properties for rapidly solidified MnAl alloys doped with C, B, and rare earth elements, J. Mater. Scien. **47** (2021) 2333-2338. https://doi.org/10.1007/s10853-011-6049-8.
13. Wannisa T., Thanida C., Panissa S., Pongsakorn J., Chesta R. and Chitnarong S. - Effects of Carbon Doping and Annealing Temperature on Magnetic MnAl Powders and MnAl Polymeric Composites, Appl. Sci. **11** (2021) 2067-2078.

    https://doi.org/10.3390/app11052067.
14. Hui D. Q., Yang Y., Jung T. L., Jong W. K., Chul J. C. and Jihoon P. - Effects of Mg and Sb Substitution on the Magnetic Properties of Magnetic Field Annealed MnBi Alloys, Nanomaterials **10** (2020) 2265-2277. https://doi.org/10.3390/nano10112265.
15. Ramakrishna V. V., Kavita S., Ramesh T., Ravi G. and Gopalan R. - On the Structural and Magnetic Properties of Mn-Bi Alloy Jet Milled at Different Feed Rates, J. Supercond. Nov. Magn. **34** (2021)733-737. https://doi.org/10.1007/s10948-020-05749-y.
16. Daniel R. B., Ke H. and Theo S. - Hard magnetic properties observed in bulk $Mn_{1-x}Ga_x$, J. Appl. Phys. **115** (2014) 17A723. https://doi.org/10.1063/1.4864141.
17. Kurt H., Rode K., Venkatesan M., Stamenov P. and Coey J. M. D. - $Mn_{3-x}Ga$ ($0 \leq x \leq 1$): Multifunctional thin film materials for spintronics and magnetic recording, Phys. Status Solidi B **248** (2011) 2338-2344. https://doi.org/10.1002/pssb.201147122.
18. Krishnan K. M. - Ferromagnetic δ-$Mn_{1-x}Ga_x$ thin films with perpendicular anisotropy, Appl. Phys. Lett. **61** (1992) 2365-2367. https://doi.org/10.1063/1.108245.
19. Ener S., Skokov K. P., Dmitriy Y. K., Michael D. K. and Oliver G. - Magnet properties of $Mn_{70}Ga_{30}$ prepared by cold rolling and magnetic field annealing, J. Magn. Magn. Mater. **382**, (2015) 265-270. https://doi.org/10.1016/j.jmmm.2015.02.001.
20. Daniel R. B., Ke H., Theo S., Tiglet B. and Rongmei N. - High Magnetic Field Annealing of Mn-Ga Intermetallic Alloys, MRS Advances **1**, (2016) 227 - 233. https://doi.org/10.1557/adv.2015.26.

21. Kharel P., Huh Y., Al-Aqtash N., Shah V .R., Sabirianov R. F., Skomski R. and Sellmyer D. J. - Structural and magnetic transitions in cubic Mn_3Ga, J. Phys.: Condens. Matter. **26** (2014) 126001. https://doi.org/10.1088/0953-8984/26/12/126001.
22. Niida H., Hori T. and Nakagawa Y. - Magnetic properties and crystal distortion of hexagonal Mn_3Ga, J. Phys. Soc. Japan. **52** (1983) 1512-1514.

https://doi.org/10.1143/JPSJ.52.1512.

23. Winterlik J., Balke B., Fecher G. H., Felser C., Alves M. C., Bernardi F. and Morais J. - Structural, electronic, and magnetic properties of tetragonal $Mn_{3-x}Ga$: Experiments and first-principles calculations, Phys. Rev. B **77** (2008) 054406. https://doi.org/10.1103/PHYSREVB.77.054406.
24. Hiroshi N., Tomiei H., Hideya O., Yasuo Y. and Yasuaki N. - Magnetization and coercivity of $Mn_{3-\delta}Ga$ alloys with a $D0_{22}$-type structure, J. Appl. Phys. **79** (1996) 5946-5948. http://dx.doi.org/10.1063/1.362115.
25. Kurt H., Rode K., Venkatesan M., Stamenov P. and Coey J. M. D. - High spin polarization in epitaxial films of ferrimagnetic Mn_3Ga, Phys. Rev. B **83** (2011) 020405-1-4. http://dx.doi.org/10.1103/PhysRevB.83.020405.
26. Balke B., Fecher G. H., Winterlik J. and Felser C. - Mn_3Ga, a compensated ferrimagnet with high Curie temperature and low magnetic moment for spin torque transfer applications, Appl. Phys. Lett. **90** (2007) 152504. https://doi.org/10.1063/1.2722206.
27. Minakuchi K., Umetsu R. Y., Ishida K. and Kainuma R. - Phase equilibria in the Mn-rich portion of Mn-Ga binary syytem, J. Alloys Comp. **537** (2012) 332-337. https://doi.org/10.1016/j.jallcom.2012.04.065.
28. Daniel R. B., Ke H., Theo S., Tiglet B. and Rongmei N. - Magnetic properties of doped Mn-Ga alloys made by mechanical milling and heat treatment, AIP Advan. **6** (2016) 056012. https://doi.org/10.1063/1.4943931.
29. Saito T. and Hamane D. N. - New hard magnetic phase in Mn-Ga-Al system alloys, J. Alloys Compd. **632** (2015) 486-489. https://doi.org/10.1016/j.jallcom.2015.01.066.
30. Sawada R., Yamamoto T., Minakuchi K., Nagasako M., Hayasaka Y., Niitsu K., Cho Y., Kainuma R. and Murakami Y. - Cellular microstructures superposed on martensite plates in $Mn_{55.2}Ga_{19.0}Cu_{25.8}$ alloy showing large coercivity, Scrip. Mater. **135** (2017) 33-36. https://doi.org/10.1016/j.scriptamat.2017.03.013.
31. Saito T. and Hamane D. N. - High coercivity in Mn-Ga-Cu alloys, AIP Advan. **6** (2016) 075004. http://dx.doi.org/10.1063/1.4958830.
32. Nazari F., Hakimi M., Mokhtari H. and Khajeh A. M. - Study of the structural and magnetic properties and gallium exchange phenomenon in a Mn-Ga alloy doped by Cr during the milling and annealing process, J. Magn. Magn. Mater. **382** (2015) 271-276. http://dx.doi.org/10.1016/j.jmmm.2015.01.084.
33. Akira K., Toshiyuki S. and Masaaki D. - Observation of hyperfine structure of $D0_{22}$-$Mn_{3-x}Fe_xGa$ by Mössbauer effect, Jpn. J. Appl. Phys. **55** (2016) 07MC04. http://doi.org/10.7567/JJAP.55.07MC04.